Accepted Manuscript

Preparation of Rhodium(III) complexes with 2(1H)-quinolinone derivatives and evaluation of their *in vitro* and *in vivo* antitumor activity

Xing Lu, Yi-Ming Wu, Jing-Mei Yang, Feng-E. Ma, Liang-Ping Li, Sheng Chen, Ye Zhang, Qing-Ling Ni, Ying-Ming Pan, Xue Hong, Yan Peng

PII: S0223-5234(18)30317-9

DOI: 10.1016/j.ejmech.2018.03.074

Reference: EJMECH 10339

To appear in: *European Journal of Medicinal Chemistry*

Received Date: 7 February 2018

Revised Date: 23 March 2018

Accepted Date: 25 March 2018

Please cite this article as: X. Lu, Y.-M. Wu, J.-M. Yang, F.-E. Ma, L.-P. Li, S. Chen, Y. Zhang, Q.-L. Ni, Y.-M. Pan, X. Hong, Y. Peng, Preparation of Rhodium(III) complexes with 2(1H)-quinolinone derivatives and evaluation of their *in vitro* and *in vivo* antitumor activity, *European Journal of Medicinal Chemistry* (2018), doi: 10.1016/j.ejmech.2018.03.074.

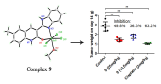

Preparation of Rhodium(III) Complexes with 2(1H)-Quinolinone Derivatives and Evaluation of Their *in Vitro* and *in Vivo* Antitumor Activity

Xing Lu[a], Yi-Ming Wu[a], Jing-Mei Yang[a], Feng-E Ma[a], Liang-Ping Li[a], Sheng Chen[a], Ye Zhang[a], Qing-Ling Ni[a], Ying-Ming Pan[a], Xue Hong[b,*], Yan Peng[a,*].

[a] *State Key Laboratory for Chemistry and Molecular Engineering of Medicinal Resources, School of Chemistry and Pharmacy, Guangxi Normal University, 15 Yucai Road , Guilin 541004, P. R. China*

[b] *State Key Laboratory of Organ Failure Research, Guangdong Provincial Institute of Nephrology Division of Nephrology, Nanfang Hospital, Southern Medical University, 1838 Guangzhou North Street, Guangzhou 510515, P. R. China*

[*]**Corresponding Authors**

Xue Hong: E-mail: hongxue0203@163.com. Phone: 086-020-62786324. Fax: 086-020-62786324.

Yan Peng: E-mail: pengyan630@aliyun.com. Phone: 086-773-2120958. Fax: 086-773-21209958.

Running title: Antitumor of Rh complexes with 2(1H)-Quinolinone derivatives

ABSTRACT

A series of 2(1H)-quinolinone derivatives and their rhodium(III) complexes were designed and synthesized. All the rhodium(III) complexes exhibited higher *in vitro* cytotoxicity for Hep G2, HeLa 229, MGC80-3, and NCI-H460 human tumor cell lines than their ligands and cisplatin, and among them complex **9** was found to be selectively cytotoxic to tumor cells. Further investigation revealed that complex **9** caused cell cycle arrest at the G2/M phase and induced apoptosis, and inhibited the proliferation of Hep G2 cells by impeding the phosphorylation of epidermal growth factor receptor (EGFR) and its downstream enzymes. Complex **9** also up-regulated the proapoptotic proteins Bak, Bax, and Bim, which altogether activated caspase-3/9 to initiate cell apoptosis. Notably, complex **9** effectively inhibited tumor growth in the NCI-H460 xenograft mouse model with less adverse effect than cisplatin.

KEYWORDS: 2(1H)-quinolinone; rhodium complex; antitumor activity; apoptosis

1. Introduction

Platinum compounds have been widely used as antitumor drugs since the discovery of cisplatin's antitumor activity by Rosenberg *et al.* [1]. However, clinically they have also shown various drawbacks, including nephrotoxicity, neurotoxicity, acquired resistance, *etc.*, and their applicability is at times limited [2–4]. As a result, new metal-based agents with fewer side effects are desired [5,6]. One of the relevant research directions focused on developing antitumor complexes of non-platinum metals [7–11]. For example, rhodium(III) complexes have recently attracted much interest due to their various pharmacology properties. Zhong *et al.* identified a rhodium(III) complex as a potent and selective NAE inhibitor that showed *in vivo* anti-inflammatory activity [12]. In addition, Yang *et al.* also reported a rhodium(III) complex that could target LSD1 and hence possessed anticancer activity [13].

Quinolines and their oxo-derivatives are known to exert biological actions such as antioxidation, anti-osteoporosis, anti-influenza, and anticancer activities [14–17]. Dovitinib, which contains the 3-substituted 2(1H)-quinolinone skeleton, has been developed as a multi-target anticancer agent and is currently under clinical investigation [18–20]. In addition, some naphthoquinone and anthraquinone derivatives were reported as multi-target antitumor agents. For example, Federica Prati *et al.* reported that the 2-phenoxy-1,4-naphthoquinones as dual molecules are able to inhibit glycolysis and mitochondrial respiration simultaneously [21], Bahia *et al.* reported that some quinonoid compounds act as antitumor agents [22], and Belluti *et al.* reported a series of quinine-coumarin hybrids as dual-targeted glyceraldehyde-3-phosphate dehydrogenase/trypanothione reductase inhibitors [23]. However, transition metal complexes derived from 3-benzimidazole-2(1H)-quinolinone have not been explored as potential antitumor

agents. In this work, as part of our continuing quest for novel metal-based anticancer agents, we designed, prepared, and characterized a series of 2(1H)-quinolinone derivatives and their rhodium(III) complexes. Among them, complex **9** showed the best *in vitro* and *in vivo* antitumor activity. The antitumor mechanism of complex **9** was carefully investigated.

2. Results and Discussion

2.1. Synthesis and Characterization

The design of the rhodium(III) complexes was based on the following consideration: 1. Both 2(1H)-quinolinone derivatives and benzimidazol derivatives are potential antitumor agents [24]. The combination of 2(1H)-quinolinone and benzimidazol may afford improved antitumor activity. 2. The combination of 2(1H)-quinolinone and benzimidazol forms bidentate ligands, which could contribute to the formation of stable metal complexes. 3. Rhodium complexes are known as potential antitumor agents. The unique geometries of rhodium complexes may lead to improved enzyme inhibition and selectivity [25].

Five 2(1H)-quinolinone derivatives bearing different substituents were synthesized. Scheme 1 shows the synthetic route for compounds **4–8**. These compounds were prepared by treating **3** with different *o*-phenylenediamine derivatives in methanol. Compound **3** was synthesized according to our reported method [14]. The structures of compounds **4–8** were characterized by NMR spectrometry and ESI-MS (Supporting Information, Figures S1−S14). Compound **4** was additionally characterized by single-crystal X-ray diffraction analysis (Figure 1). The selected bond lengths (Å) and bond angles (deg) of **4** are listed in Table S1 (Supporting Information), and the crystal data and structure refinement parameters of

4 are given in Table S2.

2.2. Crystal Structures of Rhodium Complexes

Solvothermal method is often used for the synthesis of metal complexes, in which the ligand and metal are reacted in the presence of a solvent in a sealed reactor under heating. Five rhodium complexes (complex **9–13**) were obtained by solvothermal synthesis from $RhCl_3 \cdot 3H_2O$ and compounds **4–8** in methanol and chloroform (Scheme 2), respectively, and their structure was characterized by NMR spectrometry, ESI-MS and X-ray crystallography (Figure 1, Figures S15−S29, and Table S3–S8). All these rhodium complexes were isomorphous (Figure 1). Among the five isostructural complexes, complex **9** was selected for detailed crystallographic analysis. Complex **9** had a mononuclear structure and the coordination of Rh(III) had a distorted octahedral geometry. The Rh(III) atom was chelated by a ligand and associated with three chlorine atoms and one methanol molecule. The N(3), O(1), O(2), and Cl(2) atoms formed the equatorial plane, and the two Cl(1), Cl(3) atoms were located at the apical positions. The ligand and the Rh(III) atom formed a six-membered ring by chelation. Selected bond lengths (Å) and bond angles (deg) of **9–13** are reported in Table S8, and the crystal data and structure refinement parameters of **4** are given in Table S3–S7.

2.3. Stability of Ligands and Rhodium Complexes in Solution

The stability of compounds **4**–**13** was tested under physiological conditions (PBS buffer solution containing 1% DMSO, pH = 7.3) via UV-Vis spectroscopy. All compounds were found to be stable in PBS for 24 h at room temperature based on the observations from the UV-Vis spectra (Figure S30). The stability of **4**–**13** was further tested by HPLC, and all compounds were found to be stable for 24 h in DMSO stock solution (Figure S31).

2.4. In vitro Cytotoxicity

Compounds **4**–**13** were tested against four human tumor cell lines (Hep G2, HeLa 229, MGC80-3, NCI-H460) and the normal human liver HL-7702 cells by MTT assay to evaluate their *in vitro* cytotoxicity. For comparison, the cytotoxicity of $RhCl_3 \cdot 3H_2O$ and cisplatin were also tested and used as controls. After the cells were incubated with the test compounds (2.5, 5, 10, 20, 40 μM) for 24 h, the IC_{50} values were calculated. Table 1 shows that the *in vitro* antitumor activity of the tested compound generally fell in the following order: Rh(III) complex > cisplatin > ligand > $RhCl_3 \cdot 3H_2O$. The Rh(III) complexes **9**–**13** appeared to be far more cytotoxic than $RhCl_3 \cdot 3H_2O$ for all tested cell lines, and they also showed enhanced potency in comparison with their corresponding ligand **4**–**8**. That is, a synergy that enhanced the antitumor activity took effect when the Rh(III) ion was combined with the ligands. In particular, complex **9** was more potent than cisplatin for all tested cancer cell lines but was less cytotoxic to the normal human liver HL-7702 cell line (IC_{50} = 22.8 ± 1.4 μM) than cisplatin (IC_{50} = 12.8 ± 0.9 μM). Therefore, complex **9** was selected for further detailed studies.

2.5. EGFR Inhibition

The epidermal growth factor receptor (EGFR) plays a pivotal role in cellular signaling related to cell growth, proliferation, survival, and migration. Aberrant EGFR activity is a key enabler of the development and growth of tumor cells and is associated with the onset and progression of cancer [26–31]. Therefore, we tested the inhibitory potency of **4**–**13** against wild type EGFR. The phosphorylation state of an artificial substrate, which was measured by the homogeneous time-resolved fluorescence resonance energy transfer (HTRF) method, was used as the indicator of the compounds' activity. Figure 2 shows that at the same concentration (1 μM), the

Rh(III) complexes **9**–**13** exhibited stronger inhibitory activity than their corresponding ligands **4**–**8**. Complex **9** showed an inhibition rate of 100%, the highest EGFR inhibitory activity of all tested compounds. Hence, complex **9** might be an interesting drug candidate for EGFR-driven cancer.

2.6. Western Blot Analysis of Anti-proliferative Activity against Hep G2 Cell Line

We examined the potential of complex **9** to inhibit the phosphorylation of EGFR and its downstream enzymes (Akt and Erk1/2) by Western blot analysis. Figure 3 shows that the Hep G2 cells experienced a significant reduction in EGFR phosphorylation after they were treated with complex **9** (10 μM). This result suggests that complex **9** inhibited the phosphorylation of EGFR in the Hep G2 cells.

Additionally, since the phosphorylation of Akt and ERK1/2 is required for EGFR-mediated cell proliferation, we examined the effects of complex **9** on the activation of Akt and ERK1/2. Again, it was found that the phosphorylation of Akt and ERK1/2 was inhibited by complex **9** (10 μM). Hence, complex **9** could inhibit the proliferation of Hep G2 cells by impeding the phosphorylation of EGFR and its downstream enzymes.

2.7. Gene Expression Profile

The gene expression profile is a useful for discovering cancer biomarkers and therapeutic targets [32,33]. To enhance mechanistic understandings, Hep G2 cells treated with complex **9** were examined on an Illumina Hiseq 2500 sequencing platform to measure the gene expression profile and evaluate the global changes in transcription levels. It was found that complex **9** changed the expression of 498 genes, among which 141 genes (e.g., F8, ITGB3, HIST1H2BD, E2F3) were up-regulated and 357 genes (e.g., E2F1, CCNE1, CCNB1, CCNA2) were down-regulated. Figure 4A shows the relative expression profiles of 76 genes that experienced significant

change (P < 0.5, fold change). The GO and KEGG analyses were carried out to find out relevant pathways through which target genes were significantly enriched (Figure 4B). The results suggested that complex **9** could change the expression of genes involved in cell cycle signaling in Hep G2 cells.

2.8. Cell Cycle Arrest

The Hep G2 cells were treated with complex **9** for 24 h and the cell cycle progression was measured. Figure 5 shows that compared with control group (G1: 64.61%, G2/M: 6.23%, S: 29.16%), the treated cells exhibited an accumulation in the G2/M phase, and the level of accumulation was dependent on the dose of complex **9** (1 μM, 15.19%; 2 μM, 17.54%; 5 μM, 18.46%). The results indicated G2/M phase arrest of the Hep G2 cells.

2.9. Induction of Apoptosis

The ability of complex **9** to induce apoptosis in Hep G2 cells was measured by Annexin V-PI staining and flow cytometry analyses. Figure 6 shows that after the Hep G2 cells were treated with complex **9** at 2, 5, 10 μM for 24 h, the population of early apoptotic cells increased from 5.4% in the control group to as much as 40.9%. Therefore, complex **9** is a potent apoptosis inducer.

2.10. Assessment of Caspase-3/9 Activation

Caspase-3 and caspase-9 are members of the cysteine protease family, and the sequential activation of caspases is essential in cell apoptosis. After the proapoptotic molecules activate the initiator caspase-9, caspase-9 will cleave and activate the executioner caspases-3, which results in the degradation of cellular components [34,35]. We explored whether complex **9** could activate caspase-3 and caspase-9 and consequently induce apoptosis in Hep G2 cells by treating the cells with complex **9** (5, 10, 15, 20 μM). Spectrophotometry results (Figure 7) showed that compared with the

control group, the absorbance ratio of the treated cells increased with rising dose of complex **9**. Hence, complex **9** induced cell apoptosis by activating caspase-3/9 in Hep G2 cells.

2.11. Detection of Bcl-2 protein family by Western Blot Assay

The Bcl-2 protein family consists of members that either inhibit apoptosis (e.g., Bcl-2, Bcl-xl) or promote apoptosis (e.g., Bax, Bak, Bim) [36]. Therefore, it is of interest to determine which of the Bcl-2 family proteins participated in the death signaling after cells were treated with complex **9**. The changes in the expression of candidate proteins were examined by Western blot assay. Figure 8 shows that complex **9** up-regulated the expression of Bak, Bax, and Bim in Hep G2 cells, whereas other proteins (Bcl-2, Bcl-xl) experienced no changes that were dependent on the dose of complex **9**.

2.12. Toxicological Evaluation in Mice

The toxicity of complex **9** in the mouse was evaluated extensively. Twelve male and twelve female four-week-old Kunming mice were divided randomly into four groups (n = 6). The control group received intraperitoneal saline injection once a day. The two test groups received 12.5 and 25 mg/kg body weight of intraperitoneal injection of complex **9** once a day, and the last group was treated once every two days with cisplatin at 2 mg/kg body weight. The mice were treated and monitored for the two weeks. During this time, mice treated with complex **9** showed no adverse reaction or significant loss of body weight, whereas the body weight of the mice treated with cisplatin was 13.8% less than the body weight of mice in the control group (Figure 9A). The mice were sacrificed after two weeks, and the heart, liver, and kidney were collected and weighed. Figure 9B shows that no significant change was observed in the tissues of mice treated with complex **9**. The decreased liver and kidney weights of

the mice in the cisplatin group could be attributed to their decreased body weight. The histological morphology of tissue sections was examined by haematoxylin and eosin (H&E) staining to reveal drug-related pathological changes of major organs. No significant pathological change in the heart, liver, and kidney was observed in the mice treated with complex **9**. In contrast, mice treated with cisplatin showed renal tubular injury (Figure 9C). In conclusion, complex **9** showed an acceptable safety profile since the mice tolerated treatment with it at 25 mg/kg body weight.

2.13. Growth Inhibition of NCI-H460 and Hep G2 Xenograft in Vivo

To further examine the therapeutic potential of complex **9**, we compared the antitumor efficacy of **9** and cisplatin in NCI-H460 and Hep G2 subcutaneous xenograft mice models. Tumor-bearing mice were randomly assigned and received intraperitoneal injection of complex **9**, vehicle control, or cisplatin.

Figure 10 shows that continuous treatment with complex **9** for two weeks significantly slowed the tumor growth in the NCI-H460 xenograft model. The inhibition of tumor growth was dependent on the dose of complex **9**. The relative tumor increment rate (T/C) was of 47.1% ($P < 0.01$) and 56.1% ($P < 0.05$) when the dosage was 25 and 12.5 mg/kg body weight, respectively. After the mice were sacrificed on day 14, end point tumor weight was recorded and the inhibitory rate was calculated. Complex **9** exhibited significant antitumor activity in the NCI-H460 model with an inhibitory rate of 49.8% ($P < 0.01$), lower than that of cisplatin (63.2%, $P < 0.01$).

The tumor tissues of the NCI-H460 xenograft model after treatment with complex **9** were excised for further pathological studies. The H&E-stained tissue sections of the mice treated with complex **9** and the mice in the control group showed notable differences in their tumor tissue morphology. Figure 10E shows increased necrosis in

the tumor tissues from the mice treated with complex **9** or cisplatin compared with those from the control group, and cisplatin was less effective than complex **9** to promote tumor tissues necrosis.

The Hep G2 xenograft model was also tested similarly for two weeks, and Figure S32 shows that complex **9** (25 mg/kg body weight) had a low activity on the *in vivo* growth of Hep G2 tumor (inhibitory rate: 24.0%).

In summary, the results indicated that compared with cisplatin, complex **9** was effective in inhibiting tumor growth in the NCI-H460 xenograft mouse model and incurred less adverse effect.

3. Conclusions

A series of 2(1H)-quinolinone derivatives and their rhodium(III) complexes were synthesized and characterized, and their *in vitro* antitumor activities were tested. The Rh(III) complexes showed higher cytotoxicity than their ligands and cisplatin. In particular, compared with cisplatin, complex **9** was more potent for all tested cancer cell lines and less cytotoxic to the normal human liver HL-7702 cell line. It was found that complex **9** caused cell cycle arrest at the G2/M phase and induced apoptosis, and it inhibited the proliferation of Hep G2 cells by impeding the phosphorylation of EGFR and its downstream enzymes. Complex **9** up-regulated the proapoptotic proteins Bak, Bax, and Bim, all of which helped to activate caspase-3/9 and initiate cell apoptosis. The *in vivo* tests showed that complex **9** could effectively inhibit tumor growth in the NCI-H460 xenograft mouse model, and the side effects of complex **9** were less severe than those of cisplatin. Therefore, complex **9** has the potential for further development into an efficient anticancer agent with low toxicity.

4. Experimental

4.1. Materials

All reagents and solvents were purchased from Alfa Aesar and Xilong Chemical Co., Ltd. and used directly without further purification. All compounds used in pharmacological studies had >95% purity. The HTRF kinEASE TK kit was purchased from Cisbio. The apoptosis detection kit was purchased from BD Biosciences. The caspase-3/9 assay kit was obtained from Biovision. All antibodies were purchased from Abcam. All cell lines were purchased from Shanghai Institute for Biological Science.

4.2. Instruments

Electrospray ionization mass spectrometry (ESI-MS) tests were carried out on a Bruker HCT mass spectrometer. NMR spectra were recorded on a Bruker AV-500 NMR spectrometer. HPLC analyses were carried out on an Elite P230II instrument (Dalian, China). MTT assays were performed with an M1000 microplate reader. Cell cycle analyses were performed with an FACS Aria II flow cytometer. Western blot assays were run on an ECL Western blot system. Gene expression profiles were analyzed using the Illumina Hiseq 2500 sequencing platform.

4.3. Synthesis of Ligands

A solution of **3** (1.87 g, 10 mmol) and *o*-phenylenediamine derivatives (10 mmol) in methanol (80 mL) was stirred at 65 °C for 4 h, then cooled to room temperature and filtered to give a yellow powder.

Compound **4** (yield 90%). Anal. Calc. for $C_{17}H_{13}N_3O$: C 74.17; H 4.76; N 15.26; O 5.81%, Found: C 74.13; H 4.82; N 15.22; O 5.83%. ^{1}H NMR (500 MHz, DMSO-*d6*) δ 12.65 (s, 1H), 12.40 (s, 1H), 9.00 (d, *J* = 1.7 Hz, 1H), 7.74 – 7.70 (m, 1H), 7.69 (s, 1H), 7.68 – 7.63 (m, 1H), 7.42 (d, *J* = 8.4 Hz, 1H), 7.33 (d, *J* = 8.4 Hz,

1H), 7.22 – 7.17 (m, 2H), 2.36 (s, 3H). ^{13}C NMR (125 MHz, DMSO-*d6*) δ 160.79, 147.96, 142.83, 138.90, 136.85, 134.49, 133.15, 131.89, 128.38, 122.41, 122.05, 119.93, 119.19, 118.38, 115.29, 112.88, 20.56. ESI-MS: m/z 276.11 $[M+ H]^+$.

Compound **5** (yield 88%). Anal. Calc. for $C_{19}H_{17}N_3O$: C 75.23; H 5.65; N 13.85; O 5.27%, Found: C 75.21; H 5.66; N 13.83; O 5.3%. ^{1}H NMR (500 MHz, DMSO-*d6*) δ 12.41 (s, 1H), 12.35 (s, 1H), 8.97 (s, 1H), 7.72 (s, 1H), 7.45 (s, 2H), 7.43 (d, *J* = 1.8 Hz, 1H), 7.35 (d, *J* = 8.4 Hz, 1H), 2.39 (s, 3H), 2.33 (s, 6H). ESI-MS: m/z 304.14 $[M+ H]^+$.

Compound **6** (yield 91%). Anal. Calc. for $C_{17}H_{11}F_2N_3O$: C 65.59; H 3.56; N 13.50; O 5.14%, Found: C 65.61; H 3.55; N 13.53; O 5.16%. ^{1}H NMR (500 MHz, DMSO-*d6*) δ 12.82 (s, 1H), 12.44 (s, 1H), 8.97 (s, 1H), 7.69 (s, 1H), 7.66 (d, *J* = 8.5 Hz, 2H), 7.44 (dd, *J* = 8.4, 1.6 Hz, 1H), 7.33 (d, *J* = 8.4 Hz, 1H), 2.37 (s, 3H). ^{13}C NMR (125 MHz, DMSO-*d6*) δ 160.53, 149.77, 147.79, 145.92, 138.94, 138.26, 136.83, 133.22, 131.80, 129.90, 128.35, 119.29, 118.99, 115.23, 105.46, 100.55, 20.45. ESI-MS: m/z 312.09 $[M+ H]^+$.

Compound **7** (yield 85%). Anal. Calc. for $C_{17}H_{11}Cl_2N_3O$: C 59.32; H 3.22; N 12.21; O 4.65%, Found: C 59.30; H 3.23; N 12.24; O 4.67%. ^{1}H NMR (500 MHz, DMSO-*d6*) δ 12.89 (s, 1H), 12.46 (s, 1H), 9.04 (s, 1H), 7.94 (s, 1H), 7.91 (s, 1H), 7.75 (s, 1H), 7.48 (dd, *J* = 8.4, 1.6 Hz, 1H), 7.36 (d, *J* = 8.4 Hz, 1H), 2.39 (s, 3H). ^{13}C NMR (125 MHz, DMSO-*d6*) δ 174.75, 160.98, 150.88, 142.88, 140.27, 137.51, 134.46, 133.99, 132.35, 130.10, 128.95, 124.91, 119.78, 115.74, 114.56, 99.99, 20.92. ESI-MS: m/z 342.02 $[M-H]^-$.

Compound **8** (yield 84%). Anal. Calc. for $C_{17}H_{11}Br_2N_3O$: C 47.14; H 2.56; N 9.70; O 3.69%, Found: C 47.16; H 2.57; N 9.68; O 3.71%. ^{1}H NMR (500 MHz, DMSO-*d6*) δ 12.87 (s, 1H), 12.47 (s, 1H), 9.03 (s, 1H), 8.10 (s, 1H), 8.05 (s, 1H),

7.74 (s, 1H), 7.47 (d, *J* = 9.7 Hz, 1H), 7.35 (d, *J* = 8.4 Hz, 1H), 2.39 (s, 3H). ^{13}C NMR (125 MHz, DMSO-*d6*) δ 160.95, 150.63, 143.82, 140.32, 137.49, 135.32, 133.97, 132.31, 130.08, 128.94, 122.92, 119.42, 117.68, 116.61, 116.55, 115.72, 20.93. ESI-MS: m/z 431.91 $[M-H]^-$.

4.4. Synthesis of Rh(III) Complexes

A mixture of $RhCl_3 \cdot 3H_2O$ (0.05 mmol, 0.010 g), ligand **4**–**8** (0.025 mmol), methanol (0.45 mL), and chloroform (0.15 mL) was placed in a thick Pyrex tube (*ca.* 25 cm long) and frozen by liquid N_2. The tube was vacuumed, sealed, and then heated at 80 °C for 3 days to give red block crystals suitable for X-ray diffraction analysis.

Complex **9** (yield 70%) Anal. Calc. for $C_{19}H_{21}Cl_3N_3O_3Rh$: C 41.59; H 3.86; N 7.66; O 8.75%, Found: C 41.53; H 3.82; N 7.69; O 8.71%. ^{1}H NMR (500 MHz, DMSO-*d6*) δ 14.24 (s, 1H), 14.02 (s, 1H), 9.06 (s, 1H), 8.69 (d, *J* = 8.4 Hz, 1H), 7.82 (s, 1H), 7.73 (d, *J* = 8.1 Hz, 1H), 7.70 (d, *J* = 9.5 Hz, 1H), 7.66 (d, *J* = 8.5 Hz, 1H), 7.44 (t, *J* = 7.6 Hz, 1H), 7.32 (t, *J* = 7.8 Hz, 1H), 2.49 (s, 3H). ^{13}C NMR (125 MHz, DMSO-*d6*) δ 164.60, 145.69, 142.05, 140.90, 136.40, 135.81, 135.50, 134.42, 128.74, 125.22, 122.94, 122.65, 120.92, 119.37, 117.16, 112.41, 21.06. ESI-MS: m/z 603.97 $[M+2DMSO-MeOH-Cl]^+$.

Complex **10** (yield 72%) Anal. Calc. for $C_{43}H_{54}Cl_6N_6O_7Rh_2$: C 43.57; H 4.59; N 7.09; O 9.45%, Found: C 43.55; H4.53; N 7.14; O 9.41%. ^{1}H NMR (500 MHz, DMSO-*d6*) δ 13.97 (s, 2H), 9.00 (s, 1H), 8.45 (s, 1H), 7.81 (s, 1H), 7.69 (dd, *J* = 8.6, 1.6 Hz, 1H), 7.65 (d, *J* = 8.5 Hz, 1H), 7.49 (s, 1H), 2.49 (s, 3H), 2.41 (s, 3H), 2.32 (s, 3H). ^{13}C NMR (125 MHz, DMSO-*d6*) δ 164.57, 144.58, 140.72, 140.25, 136.21, 135.54, 135.39, 134.50, 133.01, 131.60, 128.63, 122.19, 120.94, 119.57, 117.10, 112.00, 21.07, 20.86, 20.50. ESI-MS: m/z 632.01 $[M+2DMSO-MeOH-Cl]^+$.

Complex **11** (yield 68%) Anal. Calc. for $C_{39}H_{42}Cl_6F_4N_6O_7Rh_2$: C 38.99; H 3.52;

N 7.00; O 9.32%, Found: C 38.93; H3.57; N 6.92; O 9.36%. ^{1}H NMR (500 MHz, DMSO-*d6*) δ 14.56 (s, 1H), 14.06 (s, 1H), 9.05 (s, 1H), 8.64 (dd, *J* = 11.9, 7.8 Hz, 1H), 7.88 (dd, *J* = 9.9, 7.3 Hz, 1H), 7.81 (s, 1H), 7.71 (dd, *J* = 8.6, 1.7 Hz, 1H), 7.65 (d, *J* = 8.5 Hz, 1H), 2.48 (s, 3H). ^{13}C NMR (125 MHz, DMSO-*d6*) δ 163.99, 149.21, 147.22, 145.39, 140.86, 137.04, 135.98, 135.53, 135.11, 129.84, 128.30, 120.36, 118.43, 116.70, 109.27, 100.44, 20.53. ESI-MS: m/z 639.96 $[M+2DMSO-MeOH-Cl]^{+}$.

Complex **12** (yield 70%) Anal. Calc. for $C_{39}H_{41}Cl_{10}N_6O_8Rh_2$： C 36.53; H 3.22; N 6.55; O 9.98%, Found: C 36.55; H3.20; N 6.58; O 9.92%. ^{1}H NMR (500 MHz, DMSO-*d6*) δ 14.64 (s, 1H), 14.08 (s, 1H), 9.09 (s, 1H), 8.93 (s, 1H), 8.06 (s, 1H), 7.83 (s, 1H), 7.78 – 7.70 (m, 1H), 7.66 (d, *J* = 8.5 Hz, 1H), 2.49 (s, 3H). ^{13}C NMR (125 MHz, DMSO-*d6*) δ 164.52, 148.19, 141.96, 141.19, 136.60, 136.23, 135.65, 134.13, 128.87, 127.78, 125.65, 123.22, 120.83, 118.74, 117.22, 114.17, 21.05. ESI-MS: m/z 629.87 $[M+ DMSO-H]^{-}$.

Complex **13** (yield 65%) Anal. Calc. for $C_{39}H_{42}Br_4Cl_6N_6O_7Rh_2$： C 32.42; H 2.93; N 5.82; O 7.75%, Found: C 32.47; H 2.89; N 5.58; O 7.68%. ^{1}H NMR (500 MHz, DMSO-*d6*) δ 14.58 (s, 1H), 14.07 (s, 1H), 9.09 (s, 1H), 9.09 (s, 1H), 8.16 (s, 1H), 7.82 (s, 1H), 7.73 (d, *J* = 8.7 Hz, 1H), 7.66 (d, *J* = 8.5 Hz, 1H), 2.49 (s, 3H). ^{13}C NMR (125 MHz, DMSO-*d6*) δ 164.52, 147.86, 141.99, 136.62, 136.25, 135.64, 134.88, 131.04, 128.86, 126.42, 120.83, 119.71, 118.69, 117.62, 117.22, 117.12. ESI-MS: m/z 719.74 $[M+ DMSO-H]^{-}$.

4.5. X-ray Crystallography

The X-ray crystallography data of **4** and complexes **9**–**13** were collected on a Bruker SMART Apex II CCD diffractometer equipped with graphite monochromated Mo-Kα radiation (λ =0.710 73 Å) at room temperature. All crystal structures were

solved with direct methods and refined using SHELX-97 programs [37]. Tables S2–S7 list the crystallographic data of compound **4** and complexes **9–13**, and Tables S1 and S8 show selected bond lengths and bond angles.

4.6. Cell Culture and other Experimental Methods

The Hep G2, HeLa 229, MGC80-3, NCI-H460 and HL-7702 cells were obtained from Shanghai Institute for Biological Science. The cell lines were cultured in the Dulbecco's modified Eagle's medium (DMEM) supplemented with 10% fetal bovine serum (FBS). The procedures of the cytotoxicity assay, cell cycle analysis, apoptosis analysis, Western blot and *in vivo* xenograft model assay were similar to those reported by Zhang et al. [38]. The assessment of caspase-3/9 activation was performed as reported by Duan et al. [39]. The EGFR inhibition tests were performed as reported by Engel et al. [29]. The haematoxylin and eosin (H&E) staining tests were performed as reported by Guo et al.[40]. The NCI-H460 xenograft mouse models were purchased from Beijing HFK Bioscience Co., Ltd. (Beijing, China; approval No. SCXK 2014-004). The animal procedures were approved by the 181st Hospital of Chinese People's Liberation Army (Guilin, China; approval No. SYXK 2013-0004). All animal experiments were performed in accordance with the NIH guidelines for the care and use of laboratory animals. Statistical analyses were also carried out [38].

4.7. Acute Toxicity Studies

Four-week old Kunming (KM) mice (18−22 g body weight, twelve female and twelve male) were randomly divided into four groups (n = 6). Complex **9** was administered into two groups of mice at a dose of 25 and 12.5 mg/kg body weight, respectively. The mice in the control group received saline injection. The body weight of the mice was recorded daily. After treatment for two weeks, the major organs (heart,

liver, and kidney) were collected and weighed.

ACKNOWLEDGMENTS

This work was supported by the National Natural Science Foundation of China (Grants No. 81673473, 21501032). Natural Science Foundation of Guangxi Province (Grants No. 2014GXNSFAA118165, 2015GXNSFAA139010), the Innovative Team & Outstanding Talent Program of Colleges and Universities in Guangxi(2017-38) and Guangxi Natural Science Foundation of China (No. 2016GXNSFAA380300 and 2014GXNSFBA118050), State Key Laboratory for Chemistry and Molecular Engineering of Medicinal Resources (Guangxi Normal University) (CMEMR2015-A09, CMEMR2015-B12, ACMEMR2015-B10, and CMEMR2016-A09), and Guilin Scientific Research and Technology Development 1020 Project (Grant No. 20160210). Innovation Project of Guangxi Graduate Education: YCBZ2017029. Gene expression profile experiments were performed by Sheng Ting Bio-tech, Zhejiang, China.

CONFLICTS OF INTEREST

The authors declare no conflict of interest.

Supporting Information

Additional figures illustrating X-ray crystallography data, ESI-MS, NMR spectra, crystal data (CCDC No:1818157-1818162), UV-vis absorption of spectra, HPLC spectra and growth inhibition of Hep G2 xenograft *in vivo*.

REFERENCES

[1] B. Rosenberg, L. VanCamp, J.E. Trosko, V.H. Mansour, Platinum compounds: a new class of potent antitumour agents, Nature 222 (1969) 385–386.

[2] P.C. Bruijnincx, P.J. Sadler, New trends for metal complexes with anticancer activity, Curr. Opin. Chem. Biol. 12 (2008) 197–206.

[3] C.A. Rabik, M.E. Dolan, Molecular mechanisms of resistance and toxicity associated with platinating agents, Cancer Treat. Rev. 33 (2007) 9–23.

[4] M. Frezza, Q.P. Dou, Y. Xiao, H. Samouei, M. Rashidi, F. Samari, B. Hemmateenejad, In vitro and in vivo antitumor activities and DNA binding mode of five coordinated cyclometalated organoplatinum(II) complexes containing biphosphine ligands, J. Med. Chem. 54 (2011) 6166–6176.

[5] E. Gabano, M. Ravera, D. Osella, The drug targeting and delivery approach applied to pt-antitumour complexes. A coordination point of view, Curr. Med. Chem. 16 (2009) 4544–4580.

[6] F. Kratz, I.A. Muller, C. Ryppa, A. Warnecke, Prodrug strategies in anticancer chemotherapy, ChemMedChem 3 (2008) 20–53.

[7] N.P.E. Barry, P.J. Sadler, Exploration of the medical periodic table: towards new targets, Chem. Commun. 49 (2013) 5106–5131.

[8] A. Yadav, T. Janaratne, A. Krishnan, S.S. Singhal, S. Yadav, A.S. Dayoub, D.L. Hawkins, S. Awasthi, F.M. MacDonnell, Regression of lung cancer by hypoxia-sensitizing ruthenium polypyridyl complexes, Mol. Cancer Ther. 12 (2013) 643–653.

[9] A.L. Laine, C. Passirani, Novel metal-based anticancer drugs: a new challenge in drug delivery, Curr. Opin. Pharmacol. 12 (2012) 420–426.

[10] C.G. Hartinger, A.D. Phillips, A.A. Nazarov, Polynuclear ruthenium, osmium and

gold complexes. The quest for innovative anticancer chemotherapeutics, Curr. Top. Med. Chem. 11 (2011) 2688–2702.

[11] Z.F. Chen, Y.Q. Gu, X.Y. Song, Y.C. Liu, Y. Peng, H. Liang, Synthesis, crystal structure, cytotoxicity and DNA interaction of 5,7-dichloro-8-quinolinolato-lanthanides, Eur. J. Med. Chem. 59 (2013) 194–202.

[12] H.J. Zhong, W. Wang, T.S. Kang, H. Yan, Y. Yang, L. Xu, Y. Wang, D.L. Ma, C.H. Leung, A rhodium(iii) complex as an inhibitor of neural precursor cell expressed, developmentally down-regulated 8-activating enzyme with in vivo activity against inflammatory bowel disease, J. Med. Chem. 60 (2017) 497−503.

[13] C. Yang, W. Wang, J.X. Liang, G. Li, K. Vellaisamy, C.Y. Wong, D.L. Ma, C.H. Leung, A rhodium(III)-based inhibitor of lysine-specific histone demethylase 1 as an epigenetic modulator in prostate cancer cells, J. Med. Chem. 60 (2017) 2597−2603.

[14] Y. Zhang, Y.L. Fang, H. Liang, H.S. Wang, K. Hu, X.X. Liu, X.H. Yi, Y. Peng, Synthesis and antioxidant activities of 2-oxo-quinoline-3-carbaldehyde Schiff-base derivatives, Bioorg. Med. Chem. Lett. 23 (2013) 107–111.

[15] Y. Nanke, T. Kobashigawa, T. Yago, M. Kawamoto, H. Yamanaka, S. Kotake, Rebamipide, an amino acid analog of 2(1h)-quinolinone, inhibits the formation of human osteoclasts, Biomed. Res. Int. 2016 (2016) 6824719.

[16] J.N. Makau, K. Watanabe, T. Ishikawa, S. Mizuta, T. Hamada, N. Kobayashi, N. Nishida, Identification of small molecule inhibitors for influenza a virus using in silico and in vitro approaches, Plos One 12 (2017) e0173582.

[17] S. Banu, R. Bollu, R. Bantu, L. Nagarapu, S. Polepalli, N. Jain, R. Vangala, V. Manga, Design, synthesis and docking studies of novel 1,2-dihydro-4-hydroxy-2-oxoquinoline-3-carboxamide derivatives as a potential anti-proliferative agents, Eur. J. Med. Chem. 125 (2016) 400−410.

[18] A. Musolino, M. Campone, P. Neven, N. Denduluri, C.H. Barrios, J. Cortes, K. Blackwell, H. Soliman, Z. Kahan, H. Bonnefoi, M. Squires, Y. Zhang, S. Deudon, M.M. Shi, F. André, Phase II, randomized, placebo-controlled study of dovitinib in combination with fulvestrant in postmenopausal patients with HR+, HER2− breast cancer that had progressed during or after prior endocrine therapy, Breast Cancer Res. 19 (2017) 18.

[19] G.R. Petroni, B.J. Horton, C.A. Moskaluk, P.M. Fracasso, M.G. Douvas, N. Varhegyi, S. Zaja-Milatovic, C.Y. Thomas, A Phase II study of Dovitinib in Patients With Recurrent or Metastatic Adenoid Cystic Carcinoma, Clin. Cancer Res. 23 (2017) 4138−4145.

[20] S.A. Laurie, D. Hao, N.B. Leighl, J. Goffin, A. Khomani, A. Gupta, C.L. Addison, A. Bane, J. Seely, M.L. Filion, G.R. Pond, M.N. Levine, A phase II trial of dovitinib in previously-treated advanced pleural mesothelioma: the Ontario Clinical Oncology Group, Lung Cancer 104 (2017) 65−69.

[21] F. Prati, C. Bergamini, M.T. Molina, F. Falchi, A. Cavalli, M. Kaiser, R. Brun, R. Fato, M.L. Bolognesi, 2-phenoxy-1,4-naphthoquinones: from a multitarget antitrypanosomal to a potential antitumor profile, J. Med. Chem. 58 (2015) 6422-6434.

[22] S.B.B.B. Bahia, W.J. Reis, G.A.M. Jardim, F.T. Souto, C.A. de Simone, C.C. Gatto, R.F.S. Menna-Barreto, S.L. de Castro, B.C. Cavalcanti, C. Pessoa, M.H. Araujoa, E.N. da Silva Júnior, Molecular hybridization as a powerful tool towards multitarget quinoidal systems: synthesis, trypanocidal and antitumor activities of naphthoquinone-based 5-iodo-1,4-disubstituted-, 1,4- and 1,5-disubstituted-1,2,3-triazoles, Med. Chem. Comm. 7 (2016) 1555-1563.

[23] F. Belluti, E. Uliassi, G. Veronesi, C. Bergamini, M. Kaiser, R. Brun, A. Viola, R.

Fato, P.A. Michels, R.L. Krauth-Siegel, A. Cavalli, M.L. Bolognesi, Toward the development of dual-targeted glyceraldehyde-3-phosphate dehydrogenase/trypanothione reductase inhibitors against trypanosoma brucei, and trypanosoma cruzi, ChemMedChem 9 (2014) 371–382.

[24] M. Hranjec, G. Pavlović, M. Marjanović, M. Kralj, G. Karminski-Zamola, Benzimidazole derivatives related to 2,3-acrylonitriles, benzimidazo[1,2-a]quinolines and fluorenes: synthesis, antitumor evaluation in vitro and crystal structure determination, Eur. J. Med. Chem. 45 (2010) 2405–2417.

[25] C.H. Leung, H.J. Zhong, S.H. Chan, D.L. Ma, Bioactive iridium and rhodium complexes as therapeutic agents, Coordin. Chem. Rev. 257 (2013) 1764–1776.

[26] P. Chen, H. Xie, M.C. Sekar, K. Gupta, A. Wells, Epidermal growth factor receptor-mediated cell motility: phospholipase C activity is required, but mitogen-activated protein kinase activity is not sufficient for induced cell movement, J. Cell Biol. 127 (1994) 847−857.

[27] S.R. Datta, H. Dudek, X. Tao, S. Masters, H. Fu, Y. Gotoh, M.E. Greenberg, Akt phosphorylation of BAD couples survival signals to the cell-intrinsic death machinery, Cell 91 (1997) 231−241.

[28] G. Pages, P. Lenormand, G. L'Allemain, J.C. Chambard, S. Meloche, J. Pouyssegur, Mitogen-activated protein kinases p42mapk and p44mapk are required for fibroblast proliferation, Proc. Natl. Acad. Sci. U. S. A. 90 (1993) 8319−8323.

[29] J. Engel, A. Richters, M. Getlik, S. Tomassi, M. Keul, M. Termathe, J. Lategahn, C. Becker, S. Mayer-Wrangowski, C. Grütter, N. Uhlenbrock, J. Krüll, N. Schaumann, S. Eppmann, P. Kibies, F. Hoffgaard, J. Heil, S. Menninger, S. Ortiz-Cuaran, J.M. Heuckmann, V. Tinnefeld, R.P. Zahedi, M.L. Sos, C. Schultz-Fademrecht,R.K. Thomas, S.M. Kast, D. Rauh, Targeting drug resistance in EGFR with covalent

inhibitors: A structure-based design approach, J. Med. Chem. 58 (2015) 6844−6863.

[30] A. Wang, X. Li, H. Wu, F. Zou, X.E. Yan, C. Chen, C. Hu, K. Yu, W. Wang, P. Zhao, J. Wu, Z. Qi, W. Wang, B. Wang, L. Wang, T. Ren, S. Zhang, C.H. Yun, J. Liu, Q. Liu, Discovery of (R)-1-(3-(4-Amino-3-(3-chloro-4-(pyridin-2-ylmethoxy)phenyl)-1H-pyrazolo(3,4-d)pyrimidin-1-yl)piperidin-1-yl)prop-2-en-1-one (CHMFL-EGFR-202) as a Novel Irreversible EGFR Mutant Kinase Inhibitor with a Distinct Binding Mode, J. Med. Chem. 60 (2017) 2944−2962.

[31] S. Planken, D.C. Behenna, S.K. Nair, T.O. Johnson, A. Nagata, C. Almaden, S. Bailey, T.E. Ballard, L. Bernier, H. Cheng, S. Cho-Schultz, D. Dalvie, J.G. Deal, D.M. Dinh, M.P. Edwards, R.A. Ferre, K.S. Gajiwala, M. Hemkens, R.S. Kania, J.C. Kath, J. Matthews, B.W. Murray, S. Niessen, S.T. Orr, M. Pairish, N.W. Sach, H. Shen, M. Shi, J. Solowiej, K. Tran, E. Tseng, P. Vicini, Y. Wang, S.L. Weinrich, R. Zhou, M. Zientek, L. Liu, Y. Luo, S. Xin, C. Zhang, J. Lafontaine, Discovery of N-((3R,4R)-4-Fluoro-1-(6-((3-methoxy-1-methyl-1H-pyrazol-4-yl)amino)-9-methyl-9H-purin-2-yl)pyrrolidine-3-yl)acrylamide (PF-06747775) through structure-based drug design: A high affinity irreversible inhibitor targeting oncogenic EGFR mutants with selectivity over wild-type EGFR, J. Med. Chem. 60 (2017) 3002−3019.

[32] C.H. Chu, L.Y. Wang, K.C. Hsu, C.C. Chen, H.H. Cheng, S.M. Wang, C.M. Wu, T.J. Chen, L.T. Li, R. Liu, C.L. Hung, J.M. Yang, H.J. Kung, W.C. Wang, Kdm4b as a target for prostate cancer: structural analysis and selective inhibition by a novel inhibitor, J. Med. Chem. 57 (2014) 5975−5985.

[33] L.A. Salvador, K. Taori, J.S. Biggs, J. Jakoncic, D.A. Ostrov, V.J. Paul, H. Luesch, Potent elastase inhibitors from cyanobacteria: structural basis and mechanisms mediating cytoprotective and anti-inflammatory effects in bronchial

epithelial cells, J. Med. Chem. 56 (2013) 1276−1290.

[34] H. Zou, Y. Li, X. Liu, X. Wang, An APAF-1. Cytochrome c multimeric complex is a functional apoptosome that activates procaspase-9, J. Biol. Chem. 274 (1999) 11549–11556.

[35] I. Romerocanelón, L. Salassa, P.J. Sadler, The contrasting activity of iodido versus chlorido ruthenium and osmium arene azo- and imino-pyridine anticancer complexes: control of cell selectivity, cross-resistance, p53 dependence, and apoptosis pathway, J. Med. Chem. 56 (2013) 1291−300.

[36] M. Certo, V. Del Gaizo Moore, M. Nishino, G. Wei, S. Korsmeyer, S.A. Armstrong, A. Letai, Mitochondria primed by death signals determine cellular addiction to antiapoptotic BCL-2 family members, Cancer Cell 9 (2006) 351–365.

[37] G.M. Sheldrick, SHELXS97 and SHELXL97, University of Göttingen, Germany, (1997).

[38] G. Zhang, Y. An, X. Lu, H. Zhong, Y. Zhu, Y. Wu, F. Ma, J. Yang, Y. Liu, Z. Zhou, Y. Peng, Z. Chen, A novel naphthalimide compound restores p53 function in non-small-cell lung cancer by reorganizing the bak-bcl-xl complex and triggering transcriptional regulation, J. Biol. Chem. 291 (2016) 4211−4225.

[39] D. Duan, B. Zhang, J. Yao, Y. Liu, J. Fang, Shikonin targets cytosolic thioredoxin reductase to induce ROS-mediated apoptosis in human promyelocytic leukemia HL-60 cells, Free Radical Biol. Med. 70 (2014) 182−193.

[40] Z.Q. Guo, Z. Tong, B. Chen, C. Luo, S. Ouyang, S. Gong, J. Li, L.L. Mao, F. Lian, Y. Yang, Y. Huang, L. Li, J. Lu, B. Zhang, L. Zhou, H. Ding, Z. Gao, L. Zhou, G. Li, R. Zhou, K. Chen, J. Liu, Y. Wen, L. Gong, Y. Ke, S.D. Yang, X.B. Qiu, N. Zhang, J. Ren, D. Zhong, C.G. Yang, J. Liu, H. Jiang, Small-molecule targeting of E3 ligase adaptor SPOP in kidney cancer, Cancer Cell 30 (2016) 474−484.

Figure legends

Figure 1. Crystal structures of **4**, **9**–**13** with atom labeling. The free methanol in **9**–**13** is omitted for clarity.

Figure 2. Inhibition rates of **4**–**13** (1 μM) for EGFR. Afatinib (1 μM) was used as positive control.

Figure 3. (A) Complex **9** inhibits the phosphorylation of the EGFR and its downstream enzymes (Akt and Erk1/2) in Hep G2 cells. (B) Western blot bands quantified with ImageJ (from three independent measurements).

Figure 4. (A) Relative expression profiles of 76 cancer-related genes in Hep G2 cells after treatment with complex **9** (10 μM) for 24 h. (B) Gene ontology terms associated with the altered genes that show strong enrichment.

Figure 5. Cell cycle distribution of Hep G2 cells treated with complex **9** at 1, 2, 5 μM for 24 h. (A) Cell cycle arrest analysis by flow cytometry. (B) Histogram of the percentage of cells in G1, S, and G2/M phases.

Figure 6. Induction of apoptosis by complex **9** in Hep G2 cells. (A) Annexin V-PI staining and flow cytometry analysis. (B) Histogram of the percentage of early apoptotic cells.

Figure 7. Activation of (A) caspase-3 and (B) caspase-9 in Hep G2 cells treated with complex **9** (5, 10, 15, and 20 μM) for 24 h.

Figure 8. (A) Expression levels of Bcl-2 family proteins in Hep G2 cells treated with complex **9**. (B) Western blot bands quantified with ImageJ (from three independent measurements).

Figure 9. (A) Body weight of Kunming mice (n = 6) treated with complex **9** (12.5 and 25 mg/kg body weight, intraperitoneal injection once daily) or cisplatin (2 mg/kg body weight, intraperitoneal injection once every two days) for two weeks. (B) The

weight of harvested organs (heart, liver, kidney) after treatment for two weeks. (C) Histological morphology of H&E-stained tissue sections of mice in different groups.

Figure 10. *In vivo* anticancer activity of complex **9** in NCI-H460 xenograft model. (A) Body weight of nude mice treated with complex **9** (12.5 and 25 mg/kg body weight, intraperitoneal injection once daily), cisplatin (2 mg/kg body weight, intraperitoneal injection once every two days), or vehicle control (5% DMSO in saline, v/v) for 2 weeks. (B) Effect of complex **9**, cisplatin, or vehicle control on the growth of tumor xenograft. The mean tumor volume (mm^3) ± SD (n = 6) was used to indicate tumor growth and calculate the relative tumor increment rate (T/C, %). (C) Tumor weight distribution at day 14 of NCI-H460 xenograft tumors. (D) Photographs of tumor from mice in different groups. (E) Histological morphology of H&E-stained tumor tissue sections of representative nude mice in different groups.

Scheme 1. Synthesis of **4**–**8**. (a) acetic anhydride, hydrochloric acid, r.t. (b) $POCl_3$, DMF, 90 °C. (c) 70% acetic acid aqueous solution, 95 °C. (d) *o*-phenylenediamine derivatives, MeOH, 65 °C.

Scheme 2. Synthesis of the rhodium complexes. (a) $RhCl_3 \cdot 3H_2O$, MeOH/$CHCl_3$, 80 °C.

Table 1. IC_{50}[a] (μM) values of compounds **4–13** towards normal liver cell HL-7702 and four tumor cell lines.

Compound	Hep G2	HeLa229	MGC80-3	NCI-H460	HL-7702	SI Hep G2	SI HeLa229	SI MGC80-3	SI NCI-H460
4	26.6 ± 0.4	33.5 ± 1.4	22.8 ± 0.7	35.7 ± 0.7	22.8 ± 1.4	0.9	0.7	1.0	0.6
5	25.3 ± 0.6	30.1 ± 0.7	29.7 ± 0.9	33.7 ± 1.2	28.5 ± 0.9	1.1	0.9	1.0	0.8
6	>40	>40	37.5 ± 1.0	>40	>40	–	–	–	–
7	22.4 ± 1.6	26.5 ± 1.2	30.1 ± 0.5	>40	29.1 ± 0.7	1.3	1.1	1.0	–
8	20.3 ± 0.5	>40	24.7 ± 0.5	22.8 ± 0.6	30.4 ± 0.9	1.5	–	1.2	1.3
9	6.1 ± 0.2	8.4 ± 0.8	10.2 ± 0.6	6.3 ± 0.3	22.0 ± 0.7	3.6	2.6	2.2	3.5
10	8.8 ± 0.6	10.4 ± 1.2	9.4 ± 0.7	8.2 ± 1.1	13.6 ± 1.7	1.5	1.3	1.4	1.7
11	7.9 ± 0.8	11.2 ± 0.9	6.1 ± 0.5	9.6 ± 0.7	18.4 ± 1.3	2.3	1.6	3.0	1.9
12	9.6 ± 0.7	7.3 ± 0.5	10.6 ± 0.6	10.3 ± 0.8	12.5 ± 1.5	1.3	1.7	1.2	1.2
13	9.6 ± 0.7	11.5 ± 1.0	6.3 ± 0.2	10.2 ± 0.5	9.5 ± 1.2	1.0	0.8	1.5	0.9
$RhCl_3 \cdot 3H_2O$	>40	>40	>40	>40	>40	–	–	–	–

Cisplatin[b]	8.3 ± 0.6	14.5 ± 0.7	11.1 ± 0.5	17.5 ± 0.9	12.8 ± 0.9	1.5	0.9	1.2	0.7

[a] IC_{50} values are presented as the mean ± SD (standard error of the mean) from five independent experiments. [b] Cisplatin was dissolved in saline.

SI (Selectivity Index)=(IC_{50} for HL-7702)/ (IC_{50} for the respective cancer cell line)

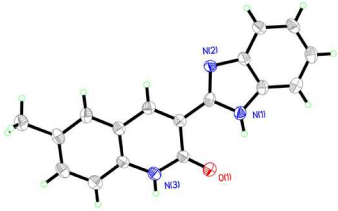

compound **4**

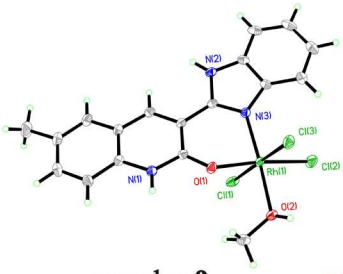

complex **9**

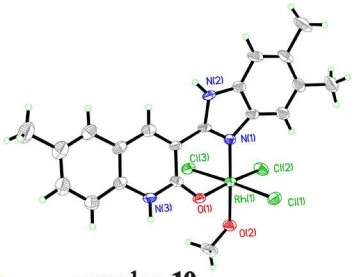

complex **10**

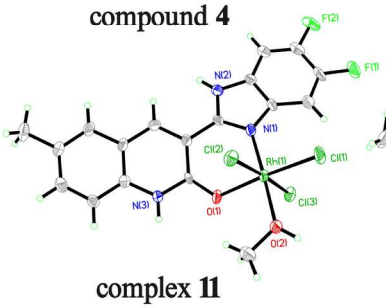

complex **11**

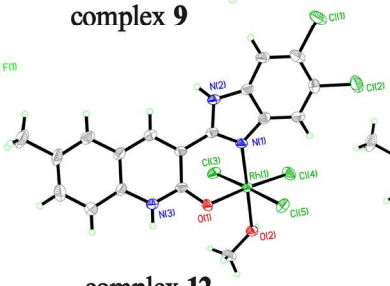

complex **12**

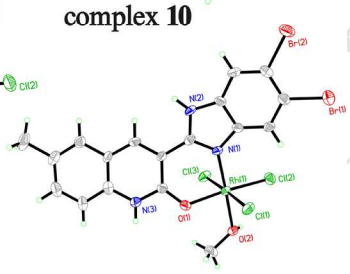

complex **13**

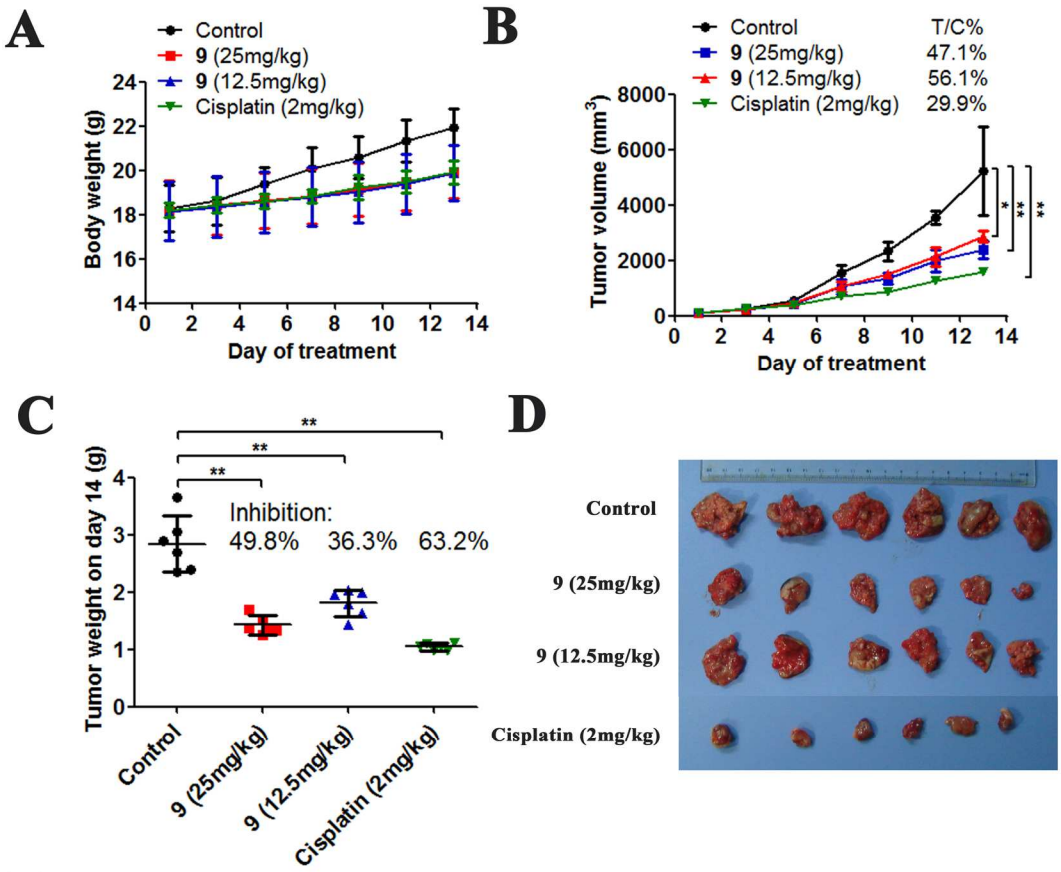
A
Control
9 (25mg/kg)
9 (12.5mg/kg)
Cisplatin (2mg/kg)
Body weight (g)
Day of treatment
B
Control T/C%
9 (25mg/kg) 47.1%
9 (12.5mg/kg) 56.1%
Cisplatin (2mg/kg) 29.9%
Tumor volume (mm3)
Day of treatment
C
Tumor weight on day 14 (g)
Inhibition:
49.8% 36.3% 63.2%
Control
9 (25mg/kg)
9 (12.5mg/kg)
Cisplatin (2mg/kg)
D
Control
9 (25mg/kg)
9 (12.5mg/kg)
Cisplatin (2mg/kg)
E
Control
9 (12.5mg/kg)
9 (25mg/kg)
Cisplatin (2mg/kg)
H&E (200X)

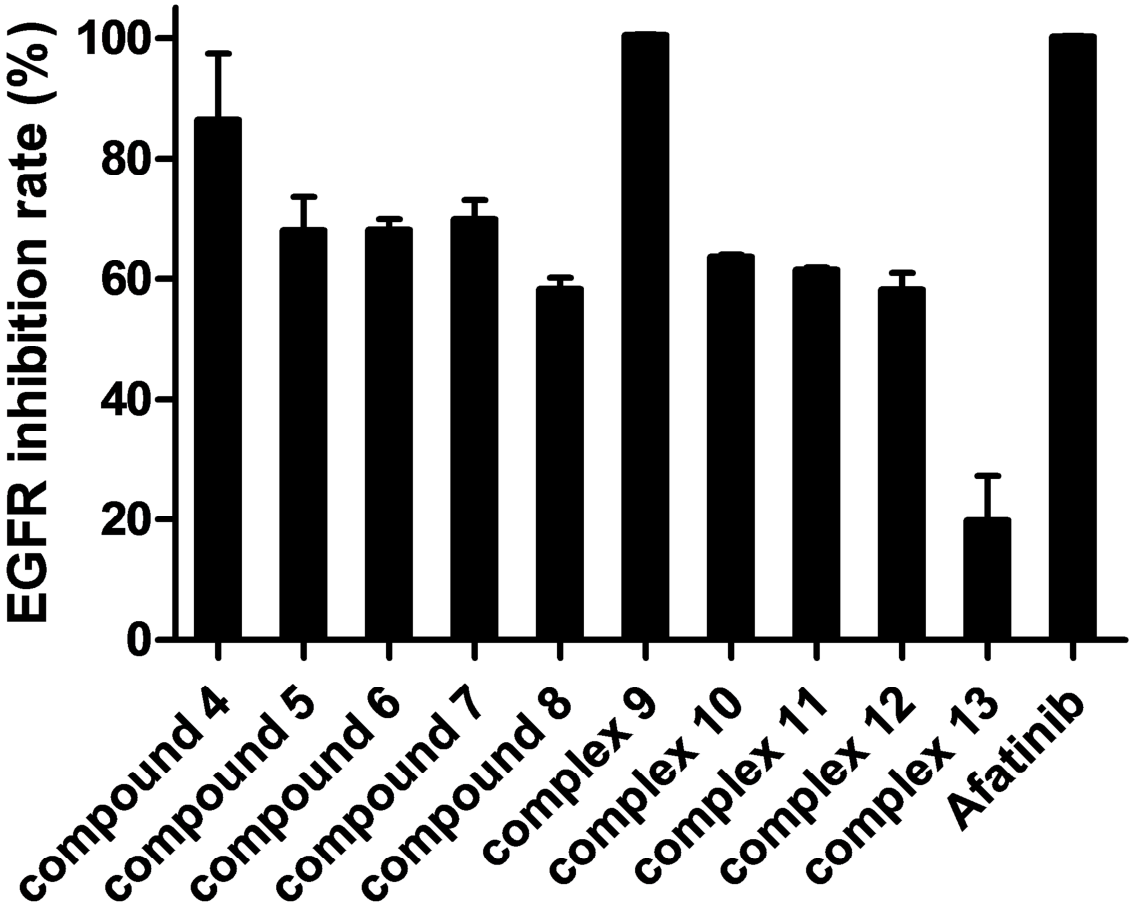
EGFR inhibition rate (%)
100
80
60
40
20
0
compound 4
compound 5
compound 6
compound 7
compound 8
complex 9
complex 10
complex 11
complex 12
complex 13
Afatinib

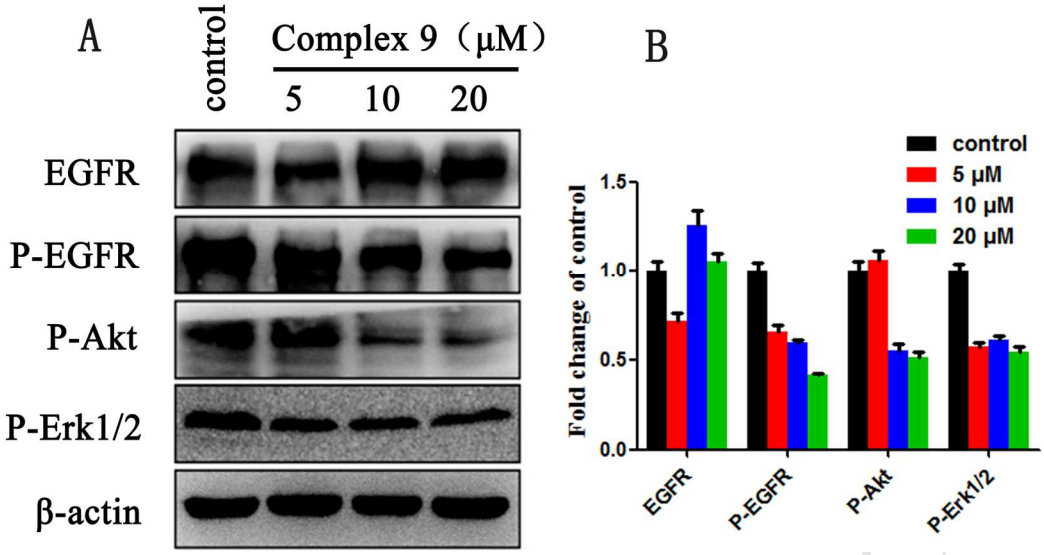

A

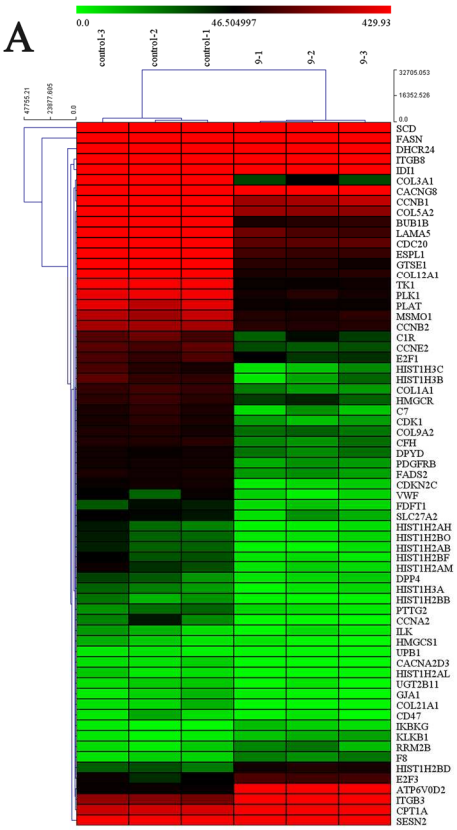

B

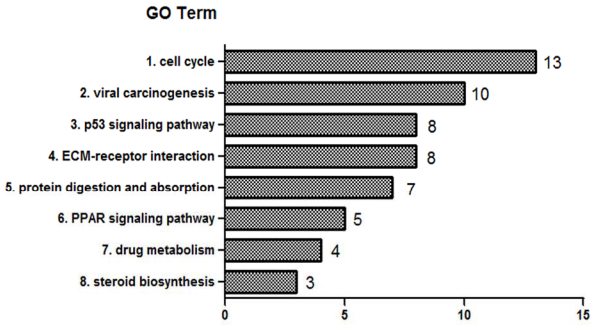

Index	Total gene count in this pathway	gene count of hits	P-Value
1	116	13	6.30E-05
2	186	10	4.73E-02
3	65	8	9.23E-04
4	79	8	2.86 E-03
5	84	7	1.33 E-02
6	63	5	4.03 E-02
7	41	4	3.57 E-02
8	16	3	1.48 E-02

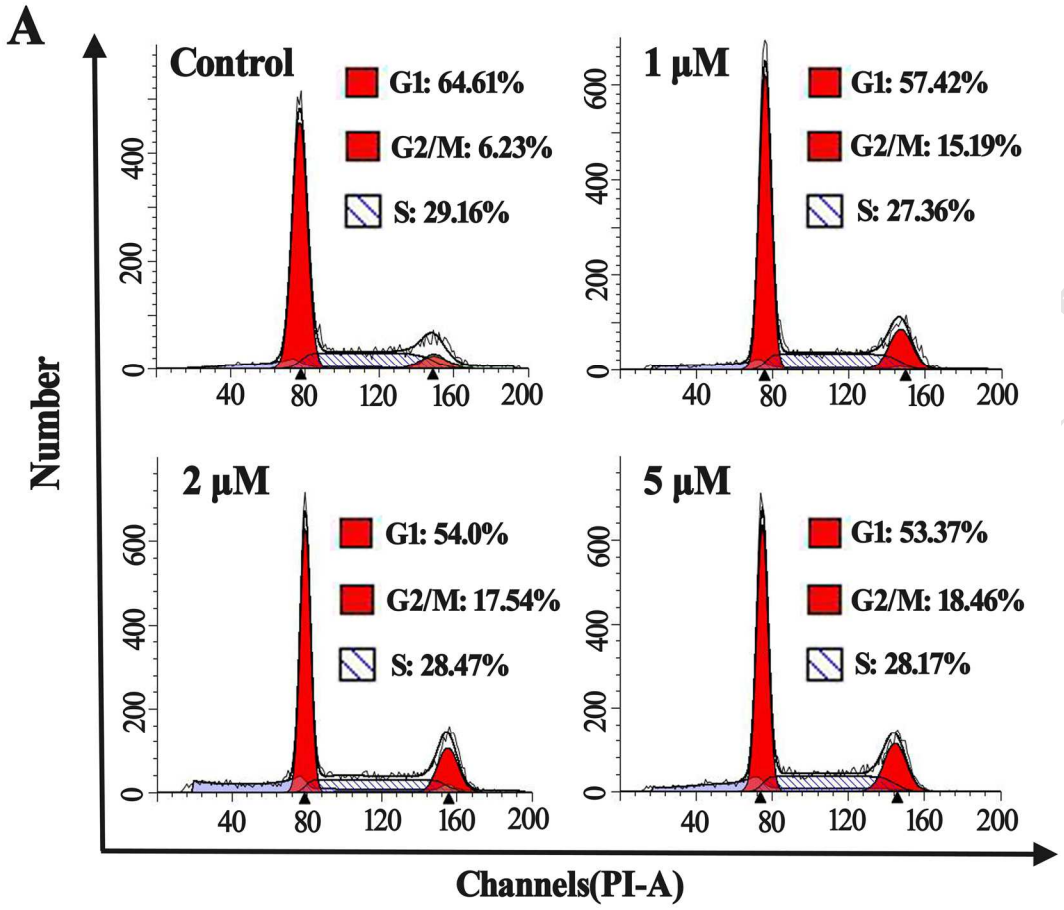
A
Control
G1: 64.61%
G2/M: 6.23%
S: 29.16%
1 μM
G1: 57.42%
G2/M: 15.19%
S: 27.36%
2 μM
G1: 54.0%
G2/M: 17.54%
S: 28.47%
5 μM
G1: 53.37%
G2/M: 18.46%
S: 28.17%
Number
Channels(PI-A)

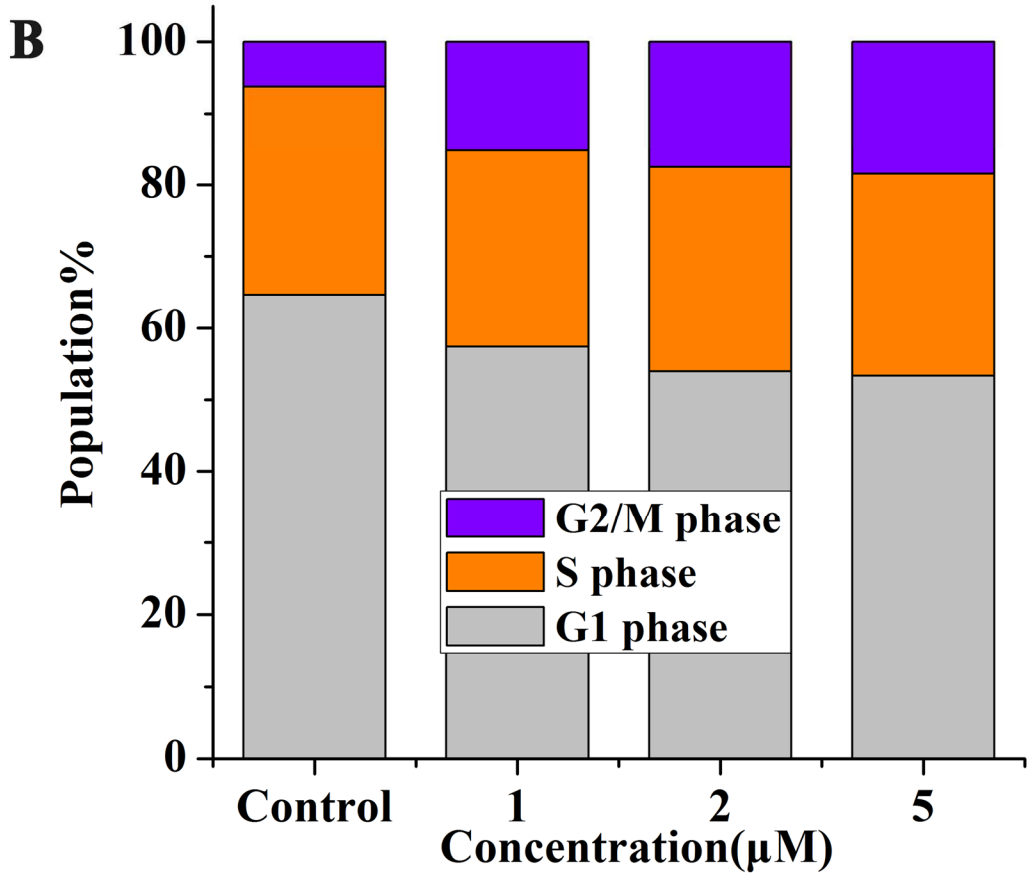
B
Population%
G2/M phase
S phase
G1 phase
Control
1
2
5
Concentration(μM)

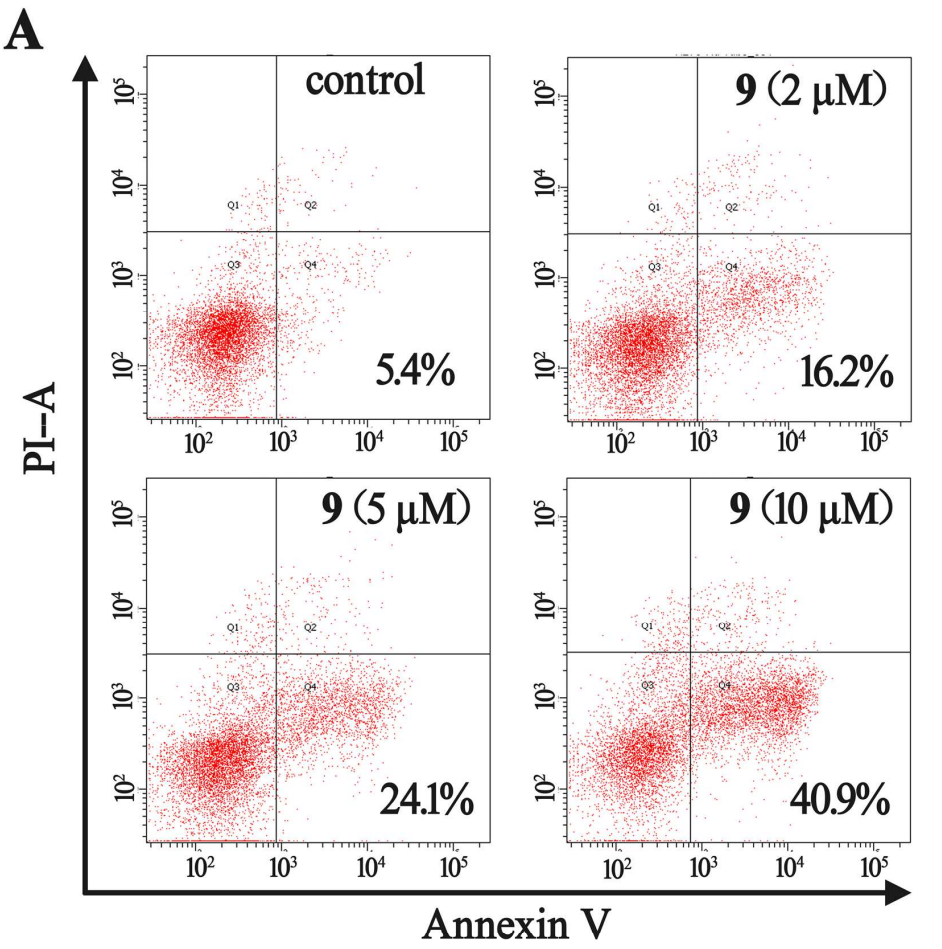
A
control
9 (2 μM)
9 (5 μM)
9 (10 μM)
5.4%
16.2%
24.1%
40.9%
PI-A
Annexin V

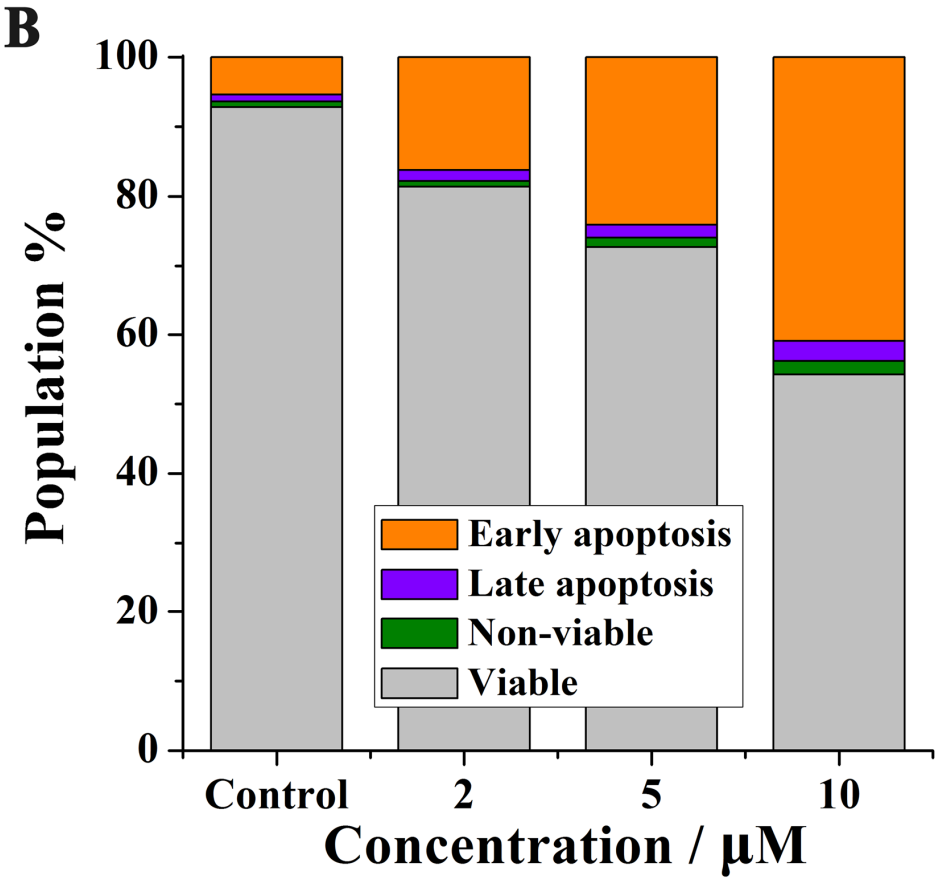
B
Population %
Early apoptosis
Late apoptosis
Non-viable
Viable
Control
2
5
10
Concentration / μM

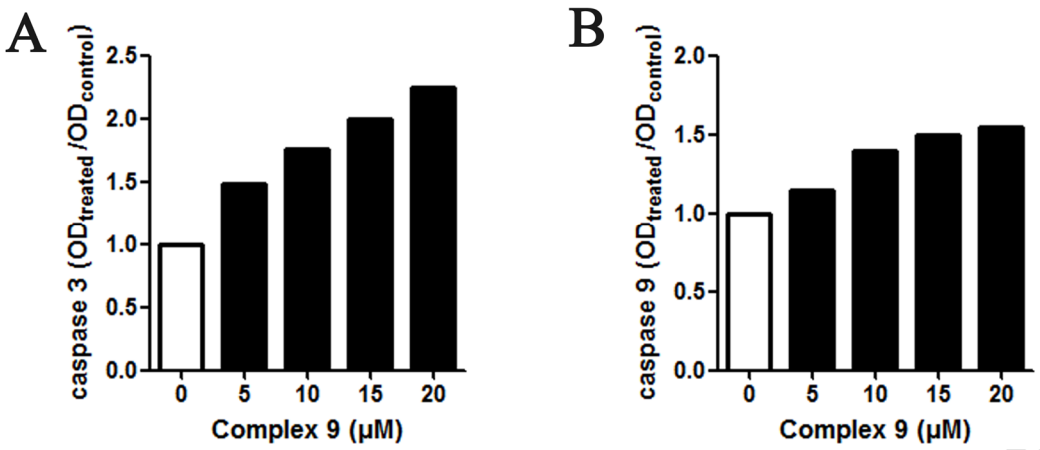

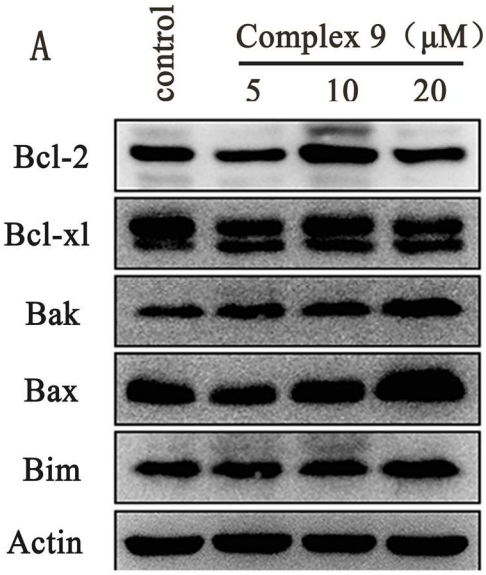

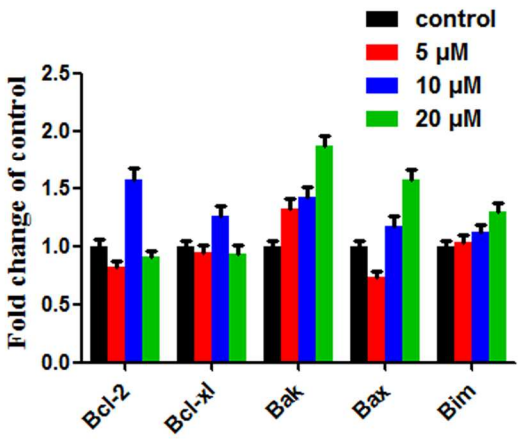

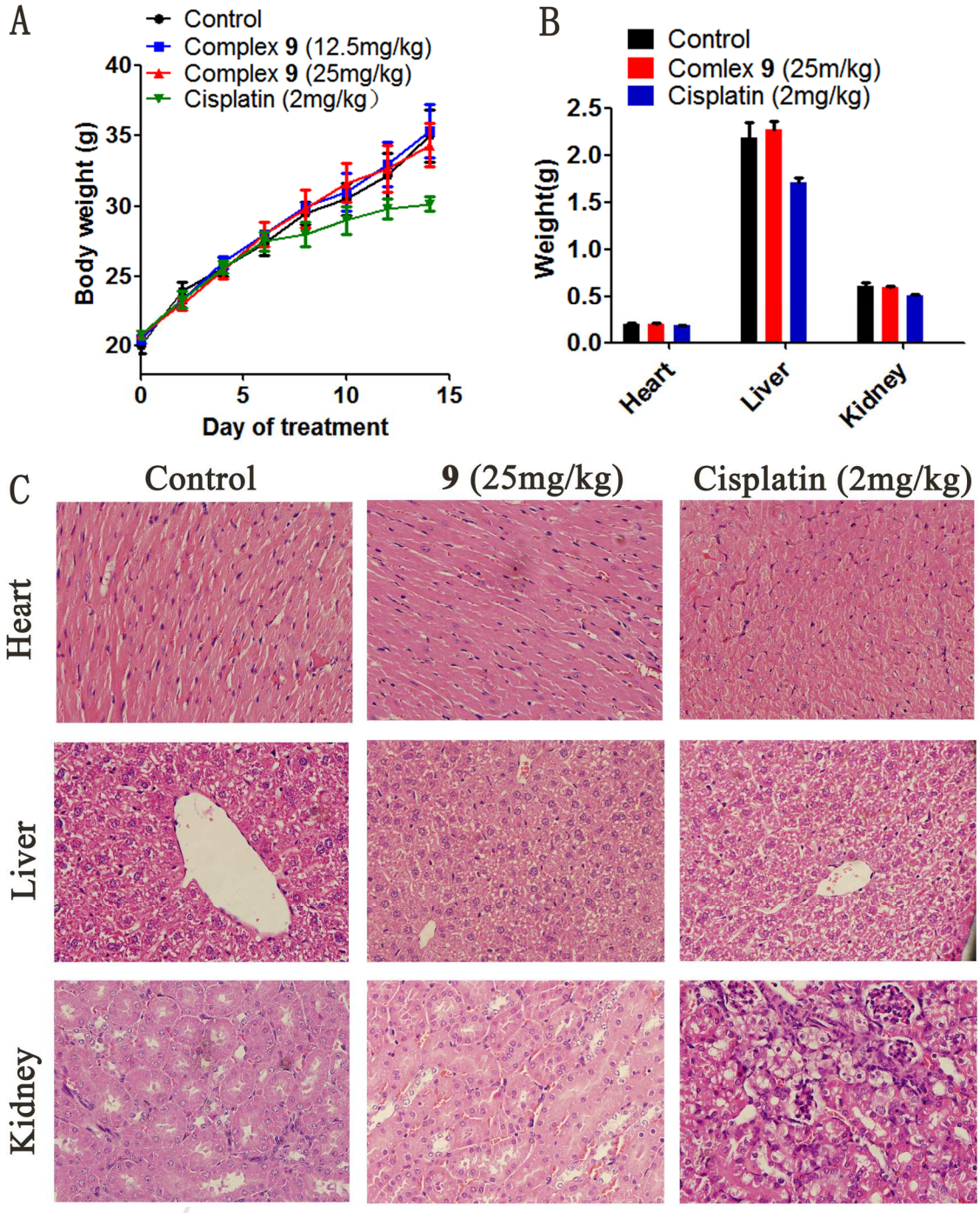
A
Control
Complex 9 (12.5mg/kg)
Complex 9 (25mg/kg)
Cisplatin (2mg/kg)
Body weight (g)
Day of treatment
B
Control
Comlex 9 (25m/kg)
Cisplatin (2mg/kg)
Weight(g)
Heart
Liver
Kidney
C
Control
9 (25mg/kg)
Cisplatin (2mg/kg)
Heart
Liver
Kidney

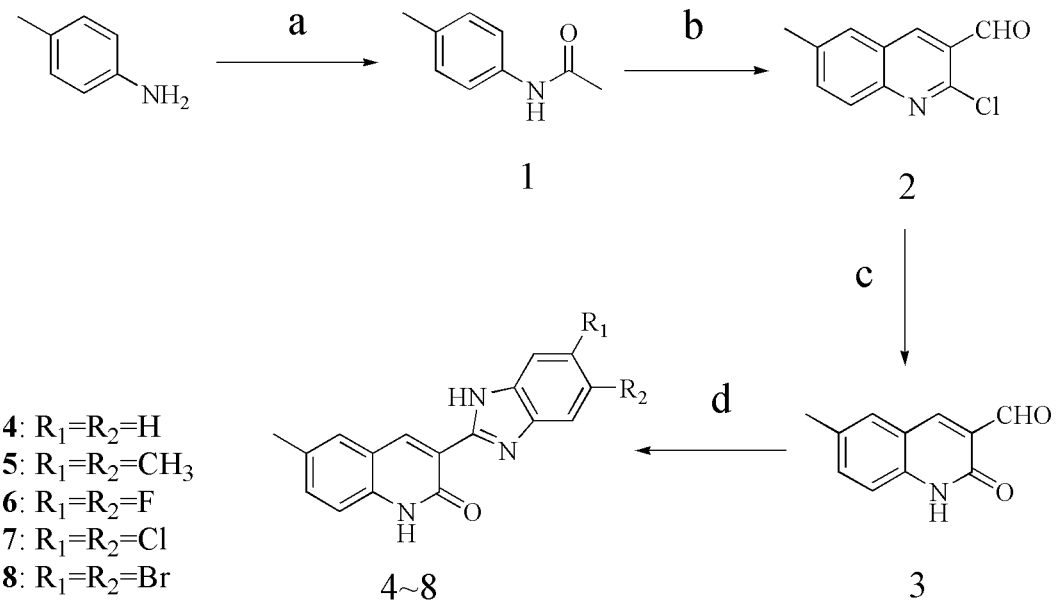

4: R_1=R_2=H
5: R_1=R_2=CH_3
6: R_1=R_2=F
7: R_1=R_2=Cl
8: R_1=R_2=Br

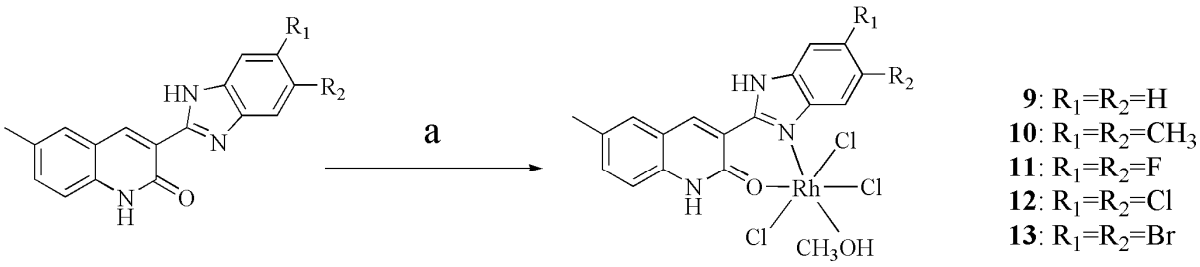

4-8

9–13

9: $R_1=R_2=H$
10: $R_1=R_2=CH_3$
11: $R_1=R_2=F$
12: $R_1=R_2=Cl$
13: $R_1=R_2=Br$

Highlights

- A series of 2(1H)-quinolinone derivatives and their rhodium(III) complexes were prepared
- Complex **9** exhibited higher *in vitro* cytotoxicity for cancer cells than cisplatin
- Complex **9** inhibited the phosphorylation of EGFR and its downstream enzymes
- Complex **9** effectively inhibited tumor growth in mice with less adverse effect than cisplatin